Effect of *p*H treatment on *K*-shell x-ray intensity ratios and *K*-shell x-ray-production cross sections in ZnCo alloys

N. Kup Aylikci,[1,*] V. Aylikci,[1] A. Kahoul,[2,3] E. Tiraşoğlu,[1] İ. H. Karahan,[4] and E. Cengiz[1]
[1]*Department of Physics, Faculty of Sciences, Karadeniz Technical University, TR-61080 Trabzon, Turkey*
[2]*Bordj-Bou-Arreridj University Center, Institute of Science and Technology, 34000, Algeria*
[3]*Physics Department, Laboratory LESIMS, Ferhat Abbas University, Faculty of Science, 19000 Setif, Algeria*
[4]*Department of Physics, Faculty of Arts and Sciences, Mustafa Kemal University, TR-31040 Hatay, Turkey*
(Received 7 June 2011; published 18 October 2011)

In this study, empirical and semiempirical *K*-shell fluorescence yields (ω_K) and $K\beta/K\alpha$ intensity ratios from the available experimental data for elements with $23 \leqslant Z \leqslant 30$ were calculated to compare them with elements in different alloys. The experimental data are fitted using the quantity $[\omega_K/(1-\omega_K)]^{1/4}$ vs Z to deduce the empirical *K*-shell fluorescence yields and $K\beta/K\alpha$ intensity ratios. The empirical and semiempirical *K*-shell fluorescence yield values were used to calculate the *K* x-ray-production cross-section values for pure Co and Zn elements. Also, $\sigma_{K\alpha}$, $\sigma_{K\beta}$ production cross sections and $K\beta/K\alpha$ intensity ratios of Co and Zn have been measured in pure metals and in different alloy compositions which have different *p*H values. The samples were excited by 59.5-keV γ rays from a ^{241}Am annular radioactive source. *K* x rays emitted by samples were counted by an Ultra-LEGe detector with a resolution of 150 eV at 5.9 keV. The effect of *p*H values on alloy compositions and the effect of alloying on the fluorescence parameters of Co and Zn were investigated. The x-ray fluorescence parameters of Co and Zn in the alloying system indicate significant differences with respect to the pure metals. These differences are attributed to the reorganization of valence shell electrons and/or charge transfer phenomena.

DOI: 10.1103/PhysRevA.84.042509 PACS number(s): 32.30.Rj

I. INTRODUCTION

Zinc and zinc alloys are widely used in the automobile industry to electroplate steel to provide corrosion resistance. The corrosion resistance of a pure zinc coating on steel is not satisfactory under severe atmospheric conditions. When elemental zinc is alloyed with iron-group metals, zinc shows better corrosion resistance than the pure metal. Thus, the investigation of properties of ZnCo alloys is interesting since these alloys exhibit a significantly higher corrosion resistance than pure zinc [1,2]. Depending on the preparation conditions, i.e., electrolyte composition, temperature, current density, and *p*H of the solution, different properties can be obtained. This fact makes ZnCo alloys important in exploring the effect of *p*H on the structure of these alloys. The effect of *p*H also changes the concentration of elements in the samples and distribution of outer shell electrons. The observed changes in the distribution of outer shell electrons lead to alteration of the binding energy of these electrons. The study of x-ray fluorescence parameters provides useful information on the electronic structure of 3*d* transition metals in their alloys and compounds. The information about the distribution of outer shell electrons is obtained by the different value of these parameters of elements in different alloy compositions since the x-ray fluorescence parameters depend on the physical and chemical environments of the elements in the samples. This dependence can be explained by the changes of the 3*d* electron population of the transition metal. The changes of the 3*d* electron population are explained by two mechanisms. The first mechanism is the transfer of valence shell electrons from one element to the other and the second is the reorganization of valence shell electrons in each atom. In alloys the 3*d* electron transfer or delocalization is responsible for the change in these parameters. Therefore it can be said that the x-ray fluorescence parameters are a sensitive tool to investigate the structure of transition metals in alloys.

The alloying effect is explained by the change of the 3*d* electron population of both elements in different alloy compositions. The change of the 3*d* electron population in the atom will modify the 3*p* orbitals more than the 2*p* orbitals which results in a change of the $K\beta$-to-$K\alpha$ ratio. In the 3*d* transition metal series, the valence state is 3*d*4*s* shells and the valence state electrons or outer shell electrons are more affected by the alloying or alien element effect than inner shell electrons. In the literature, many studies related to the effect of alloying are available and these studies are important for understanding the valence electronic structure of metals. The valence electronic structures of Fe and Ni in Fe_xNi_{1-x} alloys and of Ti, Cr, Fe, and Co in some alloys were investigated by using the changes in the relative $K\beta/K\alpha$ x-ray intensity ratio. The changes in the 3*d* electron population of elements in various alloys were explained by assuming rearrangement of electrons between 3*d* and (4*s*,4*p*) states [3–5]. Influence of the alloying effect on the *K* x-ray intensity ratio was investigated for V and Ni elements in V_xNi_{1-x} alloys. The changes in the valence electronic structure and 3*d* electron population of elements in those alloys were clarified by rearrangement and charge transfer models [6]. In addition to these studies, the alloying effect on the *K*-shell fluorescence yield was investigated for Ni in Ni-Si alloys [7] and for Cr, Ni, and Al elements in Cr_xNi_{1-x} and Cr_xAl_{1-x} alloys [8]. Electronic structures of Au-Al thin-film alloys by high-energy x-ray photoelectron spectroscopy (XPS) and x-ray absorption near-edge structure (XANES) were studied. It is concluded that the direction of charge transfer was in agreement with

*nuraykup@ktu.edu.tr

TABLE I. Solution compositions for the alloy electrodeposition.

Solution compositions	ZnCo
$ZnSO_4$ (M)	0.5
$CoSo_4$ (M)	0.1
$C_6H_5Na_3O_7{\cdot}2H_2O$ ($g\,l^{-1}$) (sodium citrate)	25
H_3BO_3 ($g\,l^{-1}$)	40
NH_4Cl ($g\,l^{-1}$)	45
Na_2SO_4 ($g\,l^{-1}$)	0.5
Solution *p*H	3, 4, 5, 6
Temperature (°C)	Room temperature
Deposition time (min)	10
Voltage (V)	–3

the differences in electronegativity values of the elements [9]. An interpretation of core-level shifts in Cu and Pd alloy compositions in terms of charge transfer between these atoms was carried out [10]. A study of high-resolution Cu L_3-edge XANES spectra for a series of Cu-Au alloys was reported. From the results of the calculations it was concluded that Cu gained *d* charge and Au lost *d* charge in the Cu-Au alloy system [11].

In this paper the effect of alloying on $K\beta$-to-$K\alpha$ x-ray intensity ratio and $K\alpha$, $K\beta$ x-ray-production cross sections has been determined. To compare the measured experimental values with pure element values, *K*-shell fluorescence yields and $K\beta/K\alpha$ intensity ratio values have been calculated empirically and semiempirically from the available experimental data. The alloying effect has been observed as the differences in the x-ray fluorescence parameters from a given element incorporated in different alloys.

II. EXPERIMENTAL PROCEDURE

A. Electrodeposition of ZnCo alloys

$Zn_{1-x}Co_x$ alloys were prepared by electrodeposition under potentiostatic conditions on aluminum substrates from a chloride sulfate plating bath at room temperature (Table I). The electrolytes were prepared using 18 MΩ-cm twice-distilled water.

The *p*H value of the bath was varied between 3 and 6 using hydrochloric acid and NaOH. The area of the deposits was 1.5 cm × 1.5 cm. The employed electrolyte was prepared using pure analytical chemicals (Merck). The counter electrode was made from platinum. The reference electrode used in all experiments was a saturated calomel electrode (SCE).

Table II shows the dependence of the Co and Zn concentrations in the films on the *p*H value of the electrolyte. Co concentration of the coatings increased with increasing bath *p*H between *p*H values 3 and 5, but further increase in the bath *p*H caused a decrease.

TABLE II. Compositions of the films.

Electrolyte *p*H	3	4	5	6
Co at. %	2.2	4.3	4.68	4
Zn at. %	97.8	95.7	95.3	96.0

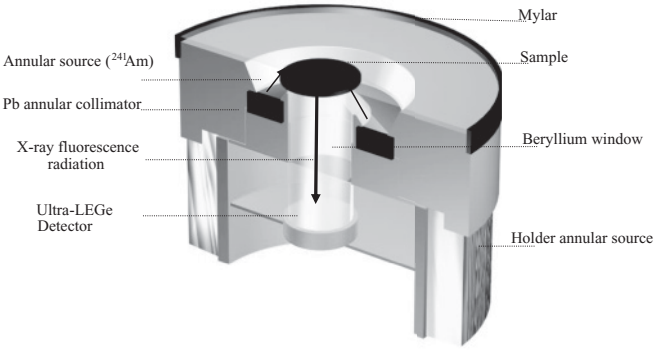

FIG. 1. Geometry of the experimental setup.

B. X-ray fluorescence analysis

The geometry of the experimental setup for the ^{241}Am annular source used in the x-ray fluorescence analysis is shown in Fig. 1. The excitation energy of the ^{241}Am is 59.6 keV. This radioisotope source was used to obtain the *K* x rays from the Co and Zn elements and the *K* x rays from the samples were detected by a collimated Ultra-LEGe detector having a thickness of 5 mm and an energy resolution of 150 eV at 5.96 keV. The spectra were analyzed by using the Origin Company (ORIGIN 7.0 demo version) software program using a least-squares fit method. In the experimental determinations, spectral deconvolution is one of the main problems that arise when determining these parameters due to the strong peak overlapping in energy dispersive x-ray fluorescence (ED-XRF) system. Good statistics are necessary for this purpose and a careful fitting methodology is required in order to obtain accurate values for the peak areas. Figures 2(a) and 2(b) show a typical Co and Zn *K* x-ray spectrum for the 14B alloy, respectively. If the figures are analyzed carefully, one can see the tailings which exist at the low-energy side of the main *K* x-ray peaks. When an electron is knocked out of the *K* shell, the reorganization of an atom is not explained by only purely radiative and nonradiative deexcitation events. Some researchers proposed that there may be an alternative decay process for filling a vacancy instead of undergoing a forbidden quadrupole transition [12,13]. In this decay process, when an inner shell hole of an atom is filled, released energy is shared between the photon and electron. It is called the radiative Auger effect. This effect can provide important information on the many-particle interaction in the atom [14]. The radiative Auger process gives rise to a satellite structure on the low-energy side of the main peak. *KMM* and *KLM* Auger peaks are found on the low-energy side of the $K\beta$ and $K\alpha$ main peaks, respectively. To obtain the proper results about the intensity ratio, cross-section and fluorescence values for the lower-energy tailing of the main peaks have to be extracted. If the tailing is not extracted from the main peak, the result can be erratic and this can be interpreted as an alloying effect or chemical effect, etc. For this purpose a fitting program was used to extract the lower-energy tailing because of the radiative Auger effect (RAE), and all the x-ray spectra were carefully analyzed and the peaks are shown in logarithmic scale. In addition to this the r^2 value can be inspected and this value is almost 0.99 for the whole range and measurements. The residue spectrum concerns the peak-determining process. If it is desired to know the main

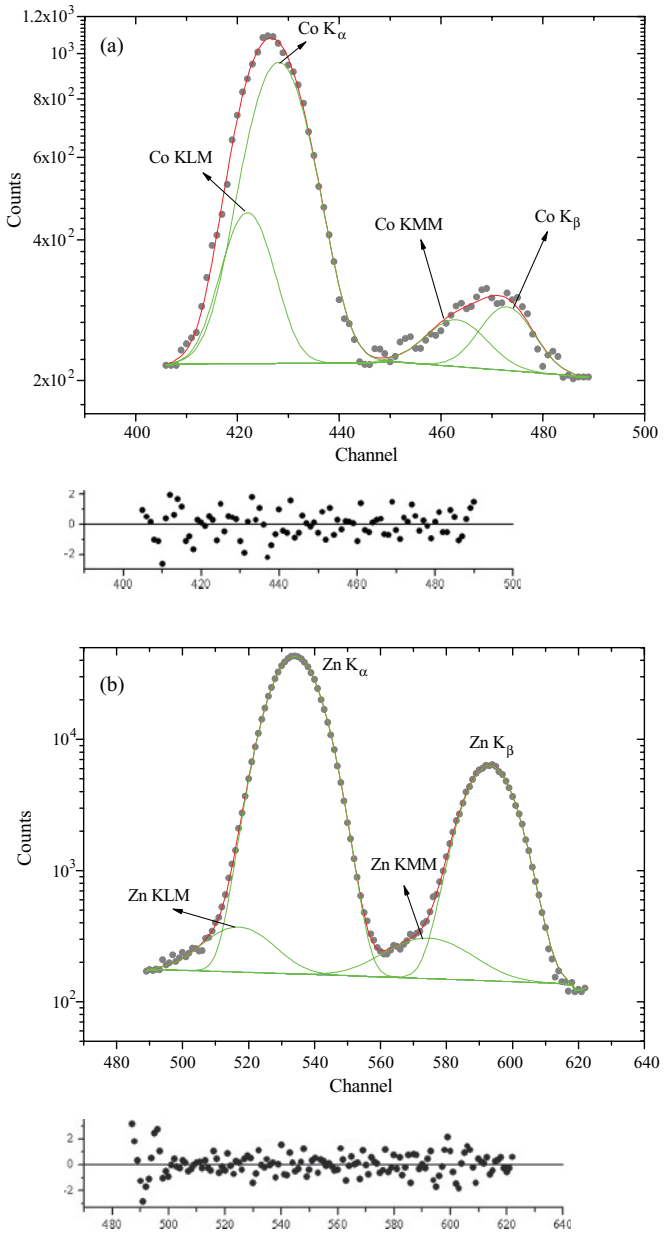

FIG. 2. (Color online) (a) Typical Co K x-ray spectrum for alloy 14B with residue spectra. (b) Typical Zn K x-ray spectrum for alloy 14B with residue spectra.

peak and the hidden peak or peaks, the residue spectra have to be checked out carefully. The residue spectra were given for Co and Zn peaks for the 14B alloy in Figs. 2(a) and 2(b).

The experimental K-shell x-ray intensity ratios K_i/K_j were evaluated using the following equation:

$$\frac{I_{Ki}}{I_{Kj}} = \frac{N_{Ki}}{N_{Kj}}\frac{\beta_{Kj}}{\beta_{Ki}}\frac{\varepsilon_{Kj}}{\varepsilon_{Ki}} \quad (i,j = \alpha,\beta), \tag{1}$$

where N_{Ki}/N_{Kj} represents the ratio of the counting rates under the K_i and K_j peak, β_{Kj}/β_{Ki} is the ratio of self-absorption correction factors of the target that accounts for the absorption of incident photons and emitted K x-ray photons, and $\varepsilon_{Kj}/\varepsilon_{Ki}$ is the ratio of the detector efficiency values for K_j and K_i x rays, respectively.

The K_i x-ray-production cross sections were obtained by using the following relation:

$$\sigma_{Ki} = \frac{N_{Ki}}{I_0 G \varepsilon_{Ki} \beta_{Ki} m_i} \quad (i = \alpha,\beta), \tag{2}$$

where N_{Ki} is the measured intensity (area under the photopeak) corresponding to the K_i x rays, I_0 is the intensity of the incident radiation, G is the geometric factor, ε_{Ki} is the detection efficiency for the K_i x rays, β_{Ki} is the self-absorption correction factor for the target material, which accounts for the absorption in the target of the incident photons and the emitted characteristic x rays, and m_i is the thickness of the target in g/cm^2.

The self-absorption correction was calculated using the equation

$$\beta_{Ki} = \frac{1 - \exp\{[-(\mu_{\rm inc}\csc\theta_1 + \mu_{\rm emt}\csc\theta_2)m_i]\}}{(\mu_{\rm inc}\csc\theta_1 + \mu_{\rm emt}\csc\theta_2)m_i}, \tag{3}$$

where $\mu_{\rm inc}$ is the mass attenuation coefficient (cm^2/g) of incident photons and $\mu_{\rm emt}$ is the mass attenuation coefficient (cm^2/g) of emitted characteristic x rays [15]. The angles of incident photons and emitted x rays with respect to the surface of the samples θ_1 and θ_2 were equal to 45° and 90° in the present experimental setup, respectively.

The product $I_0 G \varepsilon$, containing the terms related to the incident photon flux, geometrical factor, and absolute efficiency of the x-ray detector, was determined by collecting the $K\alpha$ and $K\beta$ x-ray spectra of samples of Cr, Fe, Zn, As, Se, Sr, Zr, Mo, Ru, and Cd for ^{241}Am using the equation

$$I_0 G \varepsilon_{Ki} = \frac{I_{Ki}}{\sigma_{Ki}\beta_{Ki}m_i}, \tag{4}$$

where I_{Ki} is the measured intensity (area under the photopeak) corresponding to the K_i group of x rays, I_0 is the intensity of the incident radiation, G is the geometric factor, β_{Ki} is the self-absorption correction factor for the target material, m_i is the thickness of the target in g/cm^2, and ε_{Ki} is the detection efficiency for the K_i group of x rays. The detector efficiency ε is the quantity which gives the fraction of particles being detected, i.e., the ratio of the number of particles detected per unit time to the number of particles impinging upon the detector per unit time. We calculated detector efficiency ($I_0 G \varepsilon$) values using Eq. (4) for some K x-ray energies. Then these values were plotted as a function of K x-ray energies and were fitted. We obtained two polynomial equations. Due to these equations, we obtained the values of the detector efficiency in different exciting energies. We determined detector efficiency for the energies below the Ge edge energy using Eq. (5) (for part I). Also we determined the detector efficiency for energies above the Ge edge energy using Eq. (6) (for part II):

$$Y = A + B_1X + B_2X^2 + B_3X^3 \text{ (part I)}, \tag{5}$$

$$Y = C + D_1X + D_2X^2 \text{ (part II)}, \tag{6}$$

where X is the $K\alpha$, $K\beta$ energy and the constants A, B$_1$, B$_2$, B$_3$, C, D$_1$, and D$_2$ are evaluated from the fitting polynomial. $I_0 G \varepsilon_{Ki}$ variations as a function of mean K x-ray energies are demonstrated in Fig. 3. In the photon energies which are equal and almost equal to Ge edge energy (11.102 keV) $I_0 G \varepsilon$

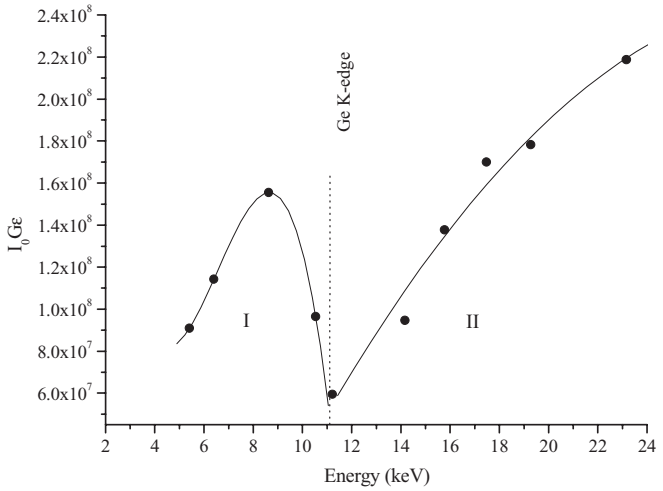

FIG. 3. The variation of the factor $I_0 G\varepsilon$ as a function of the mean K x-ray energy.

are reduced because the photons are absorbed by Ge detector crystal.

Theoretical values of σ_{Ki} x-ray-production cross sections were calculated using the following equation:

$$\sigma_{Ki} = \sigma_K(E)\omega_K F_{Ki}, \tag{7}$$

where $\sigma_K(E)$ is the K-shell photoionization cross section of the given element for the excitation energy E [16], F_{Ki} is the emission rate of the fractional x-ray for K_i x rays [17], and ω_K is the K-shell fluorescence yield that is calculated empirically and semiempirically as in the following procedure.

III. Calculation procedure of ω_K and $K\beta/K\alpha$

A. K-shell fluorescence yield ω_K

Several attempts were performed regarding the experimental determination of K-shell fluorescence yields. In this work, the well-known formula

$$[\omega_K/(1-\omega_K)]^{1/4} = \sum_i A_i Z^i \tag{8}$$

has been used which is utilized by different authors [18–23]. Taking into account this formula, empirical K-shell fluorescence yields were derived by fitting the experimental data. Then the quantity $[\omega_K/(1–\omega_K)]^{1/4}$ was calculated and was plotted vs the atomic number Z. The analytical function used for the fitting is the following polynomial:

$$\left(\frac{\omega_{K-\text{expt.}}}{1-\omega_{K-\text{expt.}}}\right)^{1/4} = \sum_{n=0}^{3} b_n Z^n \tag{9}$$

where $\omega_{K-\text{expt.}}$ is the published existing experimental data and from these values K-shell fluorescence yields can be deduced by the following formula:

$$\omega_K = \left\{\frac{[f(Z)]^4}{[1+f(Z)]^4}\right\}, \tag{10}$$

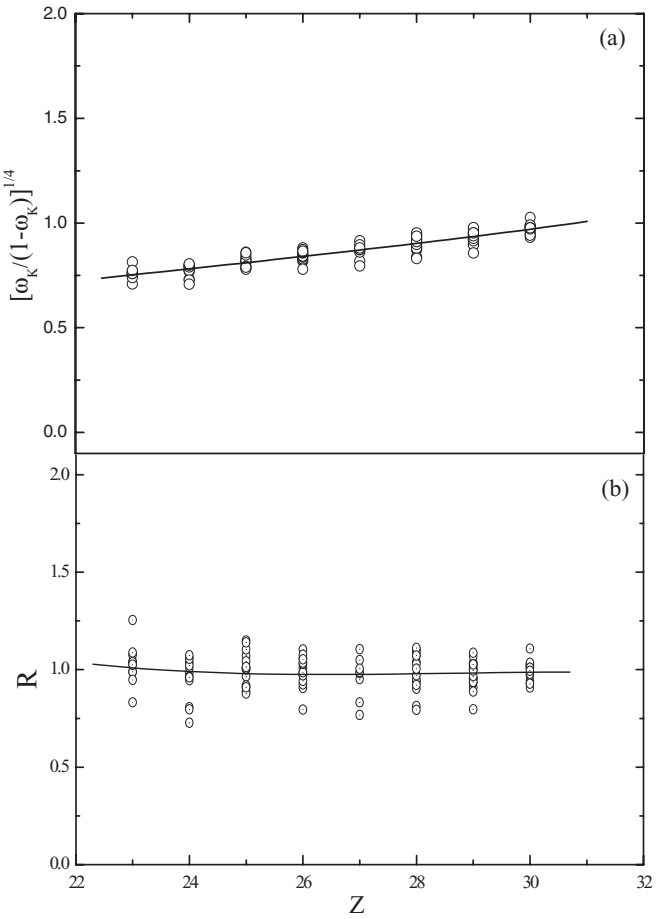

FIG. 4. (a) Distribution of experimental K-shell fluorescence yields $[\omega_K/(1-\omega_K)]^{1/4}$ as a function of atomic number. The curve is the fitting according to Eq. (9). (b) Evolution of the normalized experimental K-shell fluorescence yields as a function of atomic number. The fits are also represented by solid lines according to Eq. (13).

where $f(Z)$ is

$$f(Z) = -0.79622 + 0.13934Z - 0.0046Z^2 + 6.41077\times10^{-5}Z^3. \tag{11}$$

The experimental data $(\frac{\omega_{K-\text{expt.}}}{1-\omega_{K-\text{expt.}}})^{1/4}$ are presented in Fig. 4(a) (dots) as a function of the atomic number Z. The same figure shows the fitting results according to Eq. (9) (full lines).

For the semiempirical formula, the same published experimental data used for the calculation of empirical K-shell fluorescence yields were compared with the K-shell fluorescence yields of Krause [24] and the ratio R=$\omega_{K-\text{expt.}}/\omega_{K-\text{Krause}}$ was plotted against the atomic number Z. Then, the set of points (R, Z) was interpolated by a simple third-degree polynomial and consequently the semiempirical K-shell fluorescence yields were deduced as follows:

$$\omega_{K-S-\text{emp}} = \omega_{K-\text{Krause}} R, \tag{12}$$

where

$$R = -2.11954 + 0.3559Z - 0.01342Z^2 + 1.67184\times10^{-4}Z^3. \tag{13}$$

The fitting results are shown in Fig. 4(b).

B. $K\beta/K\alpha$ intensity ratio

The database used in this present work relies on different compilations which are available in the literature. For the calculation of K x-ray intensity ratios of elements, the empirical formula

$$\left\{\left(\frac{K\beta}{K\alpha}\right)_{\text{expt.}}\Big/\left[1-\left(\frac{K\beta}{K\alpha}\right)_{\text{expt.}}\right]\right\}^{1/4}=\sum_i A_i Z^i \qquad (14)$$

was used where $(\frac{K\beta}{K\alpha})_{\text{expt.}}$ were the existing experimental intensity ratio values. The tendency of $(\frac{K\beta}{K\alpha})$ with the atomic number Z is written by the following third-order polynomial:

$$\left(\frac{\frac{K\beta}{K\alpha}}{1-\frac{K\beta}{K\alpha}}\right)^{1/4}=\sum_{n=0}^{3} b_n Z^n. \qquad (15)$$

Using this formula, the K x-ray intensity ratio can be expressed as

$$\frac{K\beta}{K\alpha}=\left\{\frac{[g(Z)]^4}{[1+g(Z)]^4}\right\}, \qquad (16)$$

where $g(Z)$ is

$$g(Z)=1.62337-0.12744+0.00532Z^2 -7.26344\times10^{-5}Z^3. \qquad (17)$$

The fitting results are presented in Fig. 5(a) with full lines defined by Eq. (15). The dots are the experimental data.

Finally, for the determination of the semiempirical K x-ray intensity ratio formula, we calculate the semiempirical intensity ratio by means of defining the normalized experimental K x-ray intensity ratios as

$$S=\left(\frac{K\beta}{K\alpha}\right)_{\text{expt.}}\Big/\left(\frac{K\beta}{K\alpha}\right)_{\text{Scofield}}. \qquad (18)$$

The theoretical K x-ray intensity ratio was calculated by Scofield using the Hartree-Slater theory [25]. Afterwards, the normalized parameter S was plotted as a function of atomic number Z and the interpolation expression of the S parameter was obtained as follows:

$$S=5.14073-0.47052Z+0.01823Z^2-2.34525Z^3. \qquad (19)$$

The fitting results are shown in Fig. 5(b).

As a consequence of these expressions, the semiempirical K x-ray intensity ratio can be deduced by the following:

$$\left(\frac{K\beta}{K\alpha}\right)_{S-\text{expt.}}=\left(\frac{K\beta}{K\alpha}\right)_{\text{Scofield}} S. \qquad (20)$$

An eye should be kept on these proposed semiempirical and empirical formulas and their associated expressions as they are valid only within the region of $3d$ transition elements. On the contrary, these expressions will give erroneous values.

The deviation of the calculated empirical and semiempirical ω_K and $K\beta/K\alpha$ values of $3d$ transition elements from the corresponding experimental values is expressed in terms of the *root-mean-square error* (ε_{RMS}). It is calculated for each

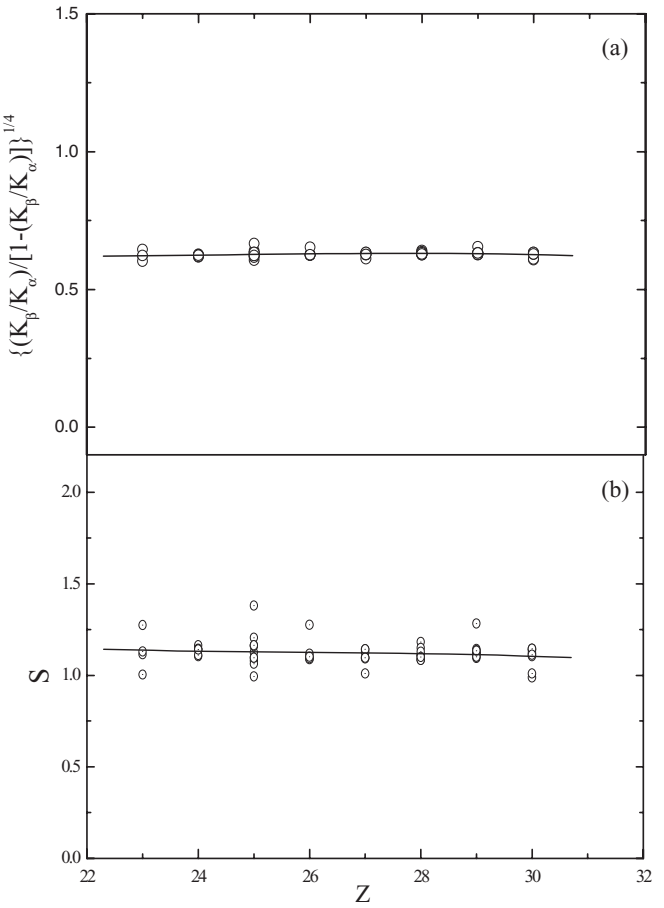

FIG. 5. (a) Distribution of experimental $(\frac{K\beta}{K\alpha})$ intensity ratio $\{(\frac{K\beta}{K\alpha})/[1-(\frac{K\beta}{K\alpha})]\}^{1/4}$ as a function of atomic number. The curve is the fitting according to Eq. (15). (b) A plot of $(\frac{K\beta}{K\alpha})_{\text{expt.}}/(\frac{K\beta}{K\alpha})_{\text{Scofield}}$ as a function of atomic number. The dots are $(\frac{K\beta}{K\alpha})_{\text{expt.}}/(\frac{K\beta}{K\alpha})_{\text{Scofield}}$ and the curve is the fitting S according to Eq. (19).

of the formulas (9), (12), (15), and (20) using the following equation:

$$\varepsilon_{RMS}=\left\{\sum_{j=1}^{N}\frac{1}{N}\left[\frac{\chi_j(\text{expt.})-\chi_j(\text{calc.})}{\chi_j(\text{calc.})}\right]^2\right\}^{1/2}, \qquad (21)$$

where N is the number of the experimental data, and χ(expt.) is the experimental ω_K for the K-shell fluorescence yields and the experimental Kβ/Kα for the intensity ratio. And finally, χ(calc.) is the calculated ω_K for the K-shell fluorescence yields and the calculated Kβ/Kα for the intensity ratio.

The calculated empirical and semiempirical ω_K and $K\beta/K\alpha$ values of $3d$ transition elements have been put in Table III with the interpolation errors. In this table, calculated empirical and semiempirical K-shell fluorescence yield values were used for the semiempirical calculation of cross-section values. Afterwards, cross-section and K x-ray intensity ratio values for pure elements were checked against the main components of alloys which were in different specimen compositions.

TABLE III. Calculated empirical and semiempirical ω_K and $K\beta/K\alpha$ values of 3*d* transition elements with the interpolation errors (ε_{RMS}).

	ω_K				$K\beta/K\alpha$			
Z	Empirical	(ε_{RMS})	Semiempirical	(ε_{RMS})	Empirical	(ε_{RMS})	Semiempirical	(ε_{RMS})
23	0.245	0.099	0.243	0.101	0.1307	0.085	0.1287	0.088
24	0.275	0.115	0.276	0.116	0.1324	0.020	0.1276	0.030
25	0.305	0.087	0.308	0.086	0.1342	0.085	0.1322	0.090
26	0.336	0.076	0.340	0.076	0.1358	0.059	0.1339	0.062
27	0.369	0.109	0.372	0.110	0.1369	0.043	0.1352	0.038
28	0.403	0.098	0.403	0.098	0.1371	0.026	0.1362	0.027
29	0.438	0.071	0.437	0.071	0.1362	0.044	0.1346	0.049
30	0.474	0.047	0.471	0.047	0.1338	0.052	0.1365	0.057

C. Evaluation of calculation procedure

To check our calculation procedure graphically, Fig. 6(a) shows the evolution of our results (empirical and semiempirical *K*-shell fluorescence yields ω_K) together those of Krause [24]. Also the results of our empirical and semiempirical intensity ratio $K\beta/K\alpha$ are presented in Fig. 6(b) together with the theoretical values reported by Scofield [25]. It is clear from Fig. 6(a) that our empirical and semiempirical *K*-shell fluorescence yields give very good agreement with Krause's values [24] for the range of elements $23 \leqslant Z \leqslant 30$ and the deviations are <1.19% for the empirical calculation, and <0.74% for the semiempirical calculation (the deviation between our values and the other calculation were calculated using the equation $D(\%) = |(\omega - \omega_{\text{emp}})/\omega_{\text{emp}}| \times 100$. For our intensity ratio $K\beta/K\alpha$ calculation, we found that our results are less satisfactory and the values of Scofield [25] are less than our calculation. We believe that this disagreement is due to the different effective weighting in the two approaches in which the spread of the experimental data is expected to be the main reason. In fact, the calculation of the semiempirical values is based on both the theoretical and the experimental values via the fitting of the *S* parameter, while for the empirical calculation only the experimental data are used, and on the other hand the theoretical calculation of Scofield is based on the Hartree-Slater theory. The deviation between our calculation and the theoretical values of Scofield [25] vary in the range of 7.25%–12.91% for the empirical intensity ratio and 9.08%–10.06% for the semiempirical calculation.

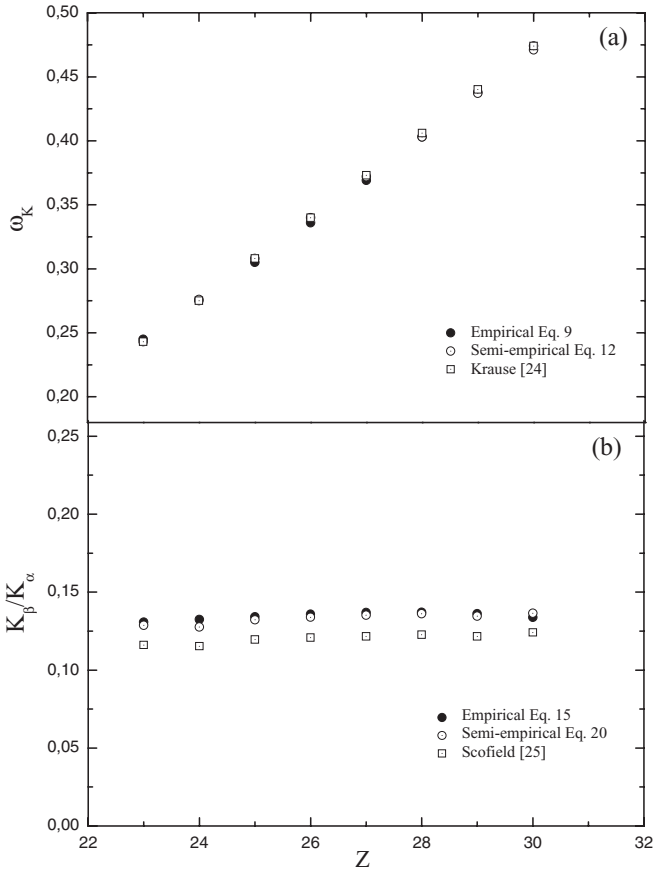

FIG. 6. (a) Empirical and semiempirical *K*-shell fluorescence yields ω_K from this work compared to those of Krause [24] as a function of the atomic number *Z*. (b) Empirical and semiempirical intensity ratio ($\frac{K\beta}{K\alpha}$) from this work compared to those of Scofield [25] as a function of the atomic number *Z*.

IV. RESULTS AND DISCUSSION

Most of the works were concerned with the effect of alloying on the changes in x-ray fluorescence parameters (*K*-shell fluorescence yields, *K* x-ray intensity ratios, etc.) or valence electronic structure of elements in different alloy

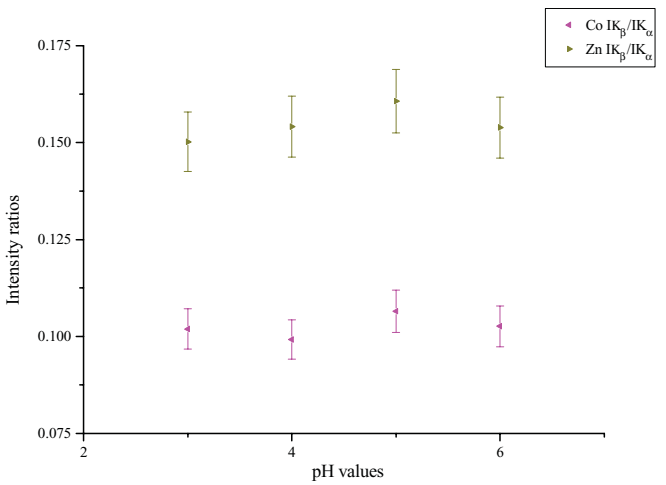

FIG. 7. (Color online) The changes in the $K\beta/K\alpha$ x-ray intensity ratio of Co and Zn.

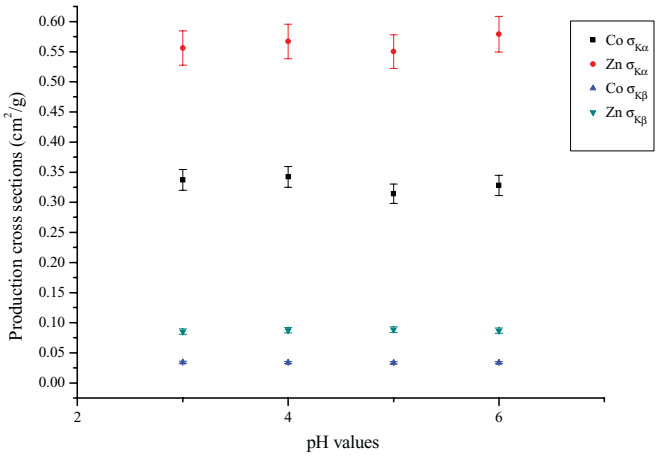

FIG. 8. (Color online) The changes in the $\sigma_{K\alpha}$ and $\sigma_{K\beta}$ values of Co and Zn.

compositions. In those studies, the alloy compositions were changed step by step and the effect of alloying was explained by means of the changes in the valence electronic structure or x-ray fluorescence parameters. But in this study the effect of pH has been investigated both on the composition of the specimen and the x-ray fluorescence parameters.

The increment of pH values, as can be seen from Table II, changes the composition of films because of the hydrogen evolution and hydrogen adsorption. During the formation of films, metallic ions are moved from anode to cathode with hydrogen and this process changes the acidity of the surroundings and the hydrogen amount. Besides, pH values change the reduction redox potential and provide metal ions for bonding to substrate material at lower potential. The other way to explain the alteration of alloy composition according to different pH values is the cathode current efficiency. The decrement of pH values (or it can be an increment of pH values for some films) reduce the cathode current efficiency and this fact causes different alloy compositions. In particular, the relationship between cathode current efficiency and pH values is the main factor for Zn alloys with Fe-like atoms.

Table II shows the dependence of Co and Zn concentrations in the films on the pH value of the electrolyte. Co concentration in the alloys increased with increasing bath pH between pH values 3 and 5, but further increasing in the bath pH caused a decrease. Since pH values change the concentration of alloys, outer shell electrons will be affected and the valence state electron distribution will change. Due to the alteration of outer shell electron distribution, K x-ray fluorescence parameters will be different in various pH values as can be seen in Figs. 7 and 8. In Fig. 8, the changes in the $\sigma_{K\alpha}$ values of Co and Zn in different pH values have been demonstrated but these values become different within experimental error limits.

The measured $K\beta/K\alpha$ x-ray intensity ratios, and the $K\alpha$ and $K\beta$ x-ray-production cross sections of Co and Zn elements in various alloy compositions of $Zn_{1-x}Co_x$ alloys are presented in Tables IV and V. Also, these parameters have been calculated empirically and semiempirically for pure $3d$ transition elements (Table III) but two different semiempirical values have been obtained in the calculation of cross-section values. The values of Co and Zn have been used to compare them in various $Zn_{1-x}Co_x$ alloys for interpreting the effect of alloying. According to our measurements, the $K\beta/K\alpha$ x-ray intensity ratio and the $K\alpha$, $K\beta$ x-ray-production cross-section values for Co and Zn in various alloy compositions are very different from the calculated empirical and semiempirical pure element values; these differences can be explained by the effect of alloying.

It is known that two or more transition metals come together to form an alloy and transition metals come together with metallic bonding. In a metallic bond, valence electrons or outer shell electrons are free to move throughout the metal or alloy. Thus, the outer shells will be more affected states than the inner shells and this fact can be seen from our measurements. If one looks through Table IV, it can be seen that the observed changes of $K\beta$ x-ray-production cross sections are more significant than $K\alpha$ x-ray, and $K\alpha$ x-ray-production cross sections are unchanged within experimental error limits. This can be explained by two reasons. First is the effective charge which is felt by the electrons and the second is open shells. The valence electronic distribution of $3d$ transition metals are

TABLE IV. The experimental $\sigma_{K\alpha}$, $\sigma_{K\beta}$ production cross sections of Co and Zn in the pure metals and in the different alloy compositions.

			$\sigma_{K\alpha}$ (cm²/g)			$\sigma_{K\beta}$ (cm²/g)		
				Calculated			Calculated	
Sample	pH values	Constitution element	Present work	Semiempirical[a]	Semiempirical[b]	Present work	Semiempirical[a]	Semiempirical[b]
Co	—	Co	0.325 ± 0.016	0.329	0.332	0.0400 ± 0.0020	0.0398	0.0402
Zn	—	Zn	0.600 ± 0.031	0.585	0.582	0.0720 ± 0.0036	0.0724	0.0719
14B	3	Co	0.337 ± 0.017	—	—	0.0343 ± 0.0017	—	—
$Zn_{0.978}Co_{0.022}$		Zn	0.566 ± 0.028	—	—	0.0851 ± 0.0043	—	—
13B	4	Co	0.342 ± 0.017	—	—	0.0339 ± 0.0017	—	—
$Zn_{0.957}Co_{0.043}$		Zn	0.567 ± 0.028	—	—	0.0874 ± 0.0044	—	—
7B	5	Co	0.314 ± 0.016	—	—	0.0334 ± 0.0017	—	—
$Zn_{0.953}Co_{0.0468}$		Zn	0.550 ± 0.028	—	—	0.0884 ± 0.0045	—	—
12B	6	Co	0.328 ± 0.016	—	—	0.0336 ± 0.0017	—	—
$Zn_{0.96}Co_{0.04}$		Zn	0.579 ± 0.029	—	—	0.0866 ± 0.0044	—	—

[a]Calculated by Eq. (7) for calculated empirical ω_K value.
[b]Calculated by Eq. (7) for calculated semiempirical ω_K value.

TABLE V. The experimental $K\beta/K\alpha$ intensity ratios of Co and Zn in the pure metals and in the different alloy compositions.

Sample	*p*H values	Constitution element	$K\beta/K\alpha$ intensity ratios						
			Present work	Calculated		Theoretical [27]	Theoretical [28]		
				Emperical	Semiemperical		Electronic configuration	Coulomb gauge	Babushkin gauge
Co	—	Co	0.1230 ± 0.0062	0.1369	0.1352	—	$3d^8 4s^1$	0.1326	0.1340
							$3d^9$	0.1304	0.1318
							$3d^8 4s^2$	0.1361	0.1374
Zn	—	Zn	0.1200 ± 0.0061	0.1338	0.1365	0.1410	—	—	—
14B	3	Co	0.1019 ± 0.0051				—	—	—
$Zn_{0.978}Co_{0.022}$		Zn	0.1502 ± 0.0076	—	—	—	—	—	—
13B	4	Co	0.0992 ± 0.0050	—	—	—	—	—	—
$Zn_{0.957}Co_{0.043}$		Zn	0.1541 ± 0.0078	—	—	—	—	—	—
7B	5	Co	0.1065 ± 0.0054	—	—	—	—	—	—
$Zn_{0.953}Co_{0.0468}$		Zn	0.1607 ± 0.0081	—	—	—	—	—	—
12B	6		0.1026 ± 0.0052	—	—	—	—	—	—
$Zn_{0.96}Co_{0.04}$		Zn	0.1539 ± 0.0078	—	—	—	—	—	—

composed of 3*d*4*s* levels. Under these levels, closed shells are formed and these inner shells feel more effective nuclear charge than outer shells. Additionally, inner shell electrons are bound more tightly than outer shells since the outer shell constitutes an open shell which is more affected by the alloying effect. The obtained $K\beta$ x-ray-production cross-section values for Co element in different alloy compositions are lower than that of two calculated semiempirical pure metal values. The changes lie between 13% and 16%. For Zn element, the changes lie between 17% and 22% and $K\beta$ x-ray-production cross-section values are higher than that of pure element values. These changes can be explained by two mechanisms. The first mechanism is the transfer of outer shell electrons from atoms of one element to atoms of the other element and the second is the rearrangement of electrons between 3*d* and (4*s*, 4*p*) states of each atom in an alloy system. It can be concluded from our results that the rearrangement mechanism cannot explain the observed changes of $K\beta$ x-ray-production cross-section values, since the rearrangement process does not cause a big change for these parameters and these changes are negligible within the experimental error limits. Thus, to faithfully explain the changes of the $K\beta$ x-ray-production cross sections of Co and Zn in different alloy compositions, the charge transfer mechanism has to be assumed.

In the case of charge transfer mechanism, the changes should be in opposite directions. The charge transfer mechanism from one element to the other can be explained by electronegativity values of Co and Zn (Table VI). Elemental Co has a bigger electronegativity value than elemental Zn and charge transfer should occur from Zn to Co. During the charge transfer from Zn to Co, the screening effect on the outer shell electrons will increase and the binding energy of the outer shell of Co will decrease. Decreasing of the binding energy of the outer shell electrons causes a decrement of *K* x-ray emission probability but the opposite effect will be observed for Zn for which the electrons are removed from it because of the lower electronegativity value.

TABLE VI. Electronegativity values of Co and Zn.

Element	*Z*	Electronegativity (Pauling scale)
Co	27	1.88
Zn	30	1.65

Similar results can be observed for $K\beta/K\alpha$ x-ray intensity ratio values. For Co, the measured experimental values are lower than the calculated empirical and semiempirical values and these changes are between 21% and 27%. On the contrary, for Zn element, $K\beta/K\alpha$ x-ray intensity ratio values are higher than that of the calculated pure element value and these changes are between 10% and 20%. Also the changes in $K\beta/K\alpha$ x-ray intensity ratio values can be explained by the charge transfer mechanism from Zn to Co but the changes are not parallel to the changes of Co or Zn concentrations in some alloy compositions. On the contrary, $K\beta$ x-ray-production

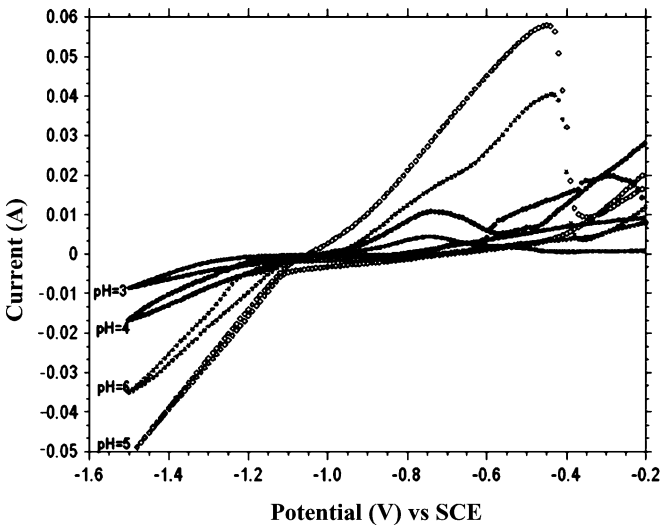

FIG. 9. Cyclic voltammograms for different *p*H values.

TABLE VII. Uncertainties in the quantities used to determine the parameters.

Quality	Nature of uncertainty	Uncertainty (%)
$N(K_i)$ $(i = \alpha, \beta, KLM, KMM)$	Counting statistic	$\leqslant 3$
$I_0 G \varepsilon_{Ki}$	Errors in different parameters used to evaluate factor	$\leqslant 2$
β	Error in the absorption coefficients at incident and emitted photon energies	$\leqslant 3$
t	Nonuniform thickness	$\leqslant 2$

cross-section values decrease vs the increment of Co concentration or increase vs the decrement of Zn concentration. There is an inverse ratio between the concentration of elements and $K\beta$ x-ray-production cross-section values. It can be seen in Table V that the increasing of pH values causes the increment of Co concentration except for 12B alloy. This alteration gives rise to a decrement of $K\beta/K\alpha$ x-ray intensity ratio compared to 14B alloy owing to the transfer of outer shell electrons from Zn to Co. For 7B alloy with a pH value of 5, Co concentration increases and this should cause a decrement of $K\beta/K\alpha$ x-ray intensity ratio with respect to 13B alloy, but it could not be observed in our measurements. The more the pH value of the alloy increases the less Co concentration we have for the 12B alloy system and Co concentration is less than the 7B alloy in the 12B alloy. Increased pH of the electrolyte (pH = 6) decreased the contents of Co in the deposits by the decrease of polarization, indicating that the deposition mechanism was governed by a normal deposition. Normal deposition describes that the reduction of polarization decreases the content of less noble metal in the deposits. In Fig. 9 it can be seen from the cyclic voltammetry curves that the increase of the electrolyte pH caused a decrease of the dissolution peak (A) except for pH = 6. This peak corresponds to the preferential dissolution of zinc, so the decrease of dissolution peaks can be related to the composition of the dissolved deposit. It can be considered that an increase in the bath pH causes a decrease in the rate of zinc deposition except pH = 4, causing the observed decrease in size of the dissolution peaks. Brenner [26] classified the electrodeposition of ZnCo alloys as anomalous. Codeposition of Zn and Co is, however, not always anomalous since at low current densities, it is possible to obtain normal deposition, where Co deposits preferentially to Zn.

A decrement of Co concentration should cause an increase of $K\beta/K\alpha$ x-ray intensity ratio value versus 12B alloy but on the contrary, the inverse effects have been fixed. The reason for this is that the decreasing of the $K\alpha$ and $K\beta$ values are in the same direction and so $K\beta/K\alpha$ x-ray intensity ratio values show reverse treatment against the decrement or increment of Co concentration.

The uncertainties in the measurements are estimated to be $<6\%$ and are found due to propagating the errors in various parameters used for determination of x-ray parameters. The uncertainties in these parameters are listed in Table VII.

To acquire more absolute results about alloying effects on the K x-ray fluorescence parameters, we plan to extend our measurements for various alloys.

V. SUMMARY AND CONCLUSIONS

In this paper, it is shown that pH values change the concentration of alloy compositions and this behavior causes an alloying effect. The effect of alloying can be seen by the changes of the K x-ray fluorescence parameters. To explain the effect of alloying, $K\alpha$, $K\beta$ x-ray-production cross-section values and $K\beta/K\alpha$ x-ray intensity ratio values were calculated empirically and semiempirically for pure elements. The comparison of measurements according to the calculated pure element value showed that outer shells were more affected than the inner shells, and the changes in the parameters could be explained by transfer of $3d$ electrons or outer shell electrons from Zn to Co since the rearrangement process did not cause a big change which is negligible within experimental error limits for these parameters.

The charge transfer mechanism was explained by the electronegativity differences between Zn and Co elements. Elemental Co has a bigger electronegativity value than Zn and the transfer of valence state electrons should go from Zn to Co. In this case, the screening effect in elemental Co will be bigger than that of Zn. The increase of screening will cause a decrease of binding energy of outer shells and thus $K\beta$ x-ray-production cross-section values will decrease for Co but will increase for Zn. A similar explanation can be made for $K\beta/K\alpha$ x-ray intensity ratio values except for elemental Co in 7B and 12B alloys, for which adverse effects have been observed vs our explanations. This fact is the result of the decrement of $K\alpha$ and $K\beta$ values in the same direction.

[1] T. Tsuru, S. Kobayashi, T. Akiyama, H. Fukushima, S. K. Gogia, and R. Kammel, J. Appl. Electrochem. **27**, 209 (1997).
[2] I. H. Karahan, Optoelectron. Adv. Mater., Rapid Commun. **2**, 828 (2008).
[3] S. Raj, H. C. Padhi, M. Polasik, F. Pawlowski, and D. K. Basa, Phys. Rev. B **63**, 073109 (2001).
[4] S. Raj, H. C. Padhi, M. Polasik, F. Pawlowski, and D. K. Basa, Solid State Commun. **116**, 563 (2000).
[5] F. Pawlowski, M. Polasik, S. Raj, H. C. Padhi, and D. K. Basa, Nucl. Instrum. Methods Phys. Res., Sect. B **195**, 367 (2002).
[6] S. Raj, H. C. Padhi, and M. Polasik, Nucl. Instrum. Methods Phys. Res. Sect. B **155**, 143 (1999).
[7] Y. Kalayci, Y. Agus, S. Ozgur, N. Efe, A. Zararsiz, P. Arikan, and R. H. Mutlu, Spectrochim. Acta, Part B **60**, 277 (2005).
[8] E. Buyukkasap, Spectrochim. Acta, Part B **53**, 499 (1998).

[9] H. Piao, N. S. McIntyre, G. Beamson, M.-L. Abel, and J. F. Watts, J. Electron Spectrosc. **125**, 35 (2002).
[10] R. J. Cole, N. J. Brooks, and P. Weightman, Phys. Rev. B **56**, 12178 (1997).
[11] T. K. Sham, A. Hiraya, and M. Watanabe, Phys. Rev. B **55**, 7585 (1997).
[12] F. Bloch and P. A. Ross, Phys. Rev. **47**, 884 (1935).
[13] F. Bloch, Phys. Rev. **48**, 187 (1935).
[14] A. Mühleisen, M. Budnar, and J.-Cl. Dousse, Phys. Rev. A **54**, 3852 (1996).
[15] M. J. Berger and J. H. Hubbell, XCOM: Photon cross sections on a personnel computer (version 1.2), NBSIR85-3597, National Bureau of Standards, Gaithersburg, MD, USA. For version 3.1, 1999, see [http://physics.nist.gov/].
[16] H. Scofield, Lawrence Livermore National Laboratory Report UCRL-51326 (1973), .
[17] N. Broll, X-Ray Spectrom. **15**, 271 (1986).
[18] M. Has, Ann. Phys. **5**, 16 473 (1932).
[19] E. Arends, Ann. Phys. **22**, 281 (1935).
[20] P. R. Gray, Phys. Rev. **101**, 1306 (1956).
[21] E. H. S. Burhop and J. Phys, Radium **16**, 625 (1955).
[22] V. O. Kostroun, M. H. Chen, and B. Crasemann, Phys. Rev. A **4**, 429 (1971).
[23] A. Kahoul, A. Abassi, B. Deghfel, and M. Nekkab, Radiat. Phys. Chem. **80**, 369 (2011).
[24] M. O. Krause, J. Phys. Chem. Ref. Data **8**, 307 (1979).
[25] J. H. Scofield, At. Data Nucl. Data Tables **14**, 121 (1974).
[26] A. Brenner, *Electrodeposition of Alloys* (Academic Press, New York, 1963), Vol. II.
[27] J. H. Scofield, Phys. Rev. A **9**, 1041 (1973).
[28] M. Polasik, Phys. Rev. A **58**, 1840 (1998).